Multiple Sector ID Capture (MIDC): A Novel Beamforming Technique for 60-GHz Band Multi-Gbps WLAN/PAN Systems

Ken'ichi Hosoya, *Member, IEEE*,
Narayan Prasad, Kishore Ramachandran, Naoyuki Orihashi, Shuya Kishimoto, *Member, IEEE*,
Sampath Rangarajan, *Senior Member, IEEE*, and Kenichi Maruhashi, *Member, IEEE*

***Abstract*—A novel beamforming (BF) technique (MIDC: Multiple sector-ID Capture) is proposed for 60-GHz band WLAN/PAN systems. In contrast to conventional BF techniques adopted in 60-GHz band standards, where quasi-omni (Q-omni) antenna radiation patterns are utilized, MIDC precisely detects the best link even when the Q-omni pattern is imperfect. Furthermore, it can reserve multiple antenna settings corresponding to existing communication links in the initial training by making use of the quasi-optical nature of millimeter-waves. This enables fast beam switching when link blockage occurs. The training is executed in short durations by putting together DoA/DoD-estimation and "beam-combining" techniques. The basic function of MIDC is verified experimentally in a simple multipath propagation environment by using our 60-GHz CMOS transceiver LSIs integrated with planar phased-array antennas. MIDC has been adopted in the MAC/PHY specification of the primary 60-GHz band standards: WiGig (Wireless Gigabit Alliance) and IEEE 802.11ad.**

***Index Terms*—Beam steering, CMOS integrated circuits, millimeter wave propagation, phased arrays, wireless LAN.**

I. Introduction

THE unlicensed 60-GHz frequency band available in principal countries of the world has activated research and development on multi-Gbps wireless systems exploiting its extensive frequency resources up to 9 GHz [1], [2]. Various standardization activities such as Wireless Gigabit Alliance (WiGig [3], now unified with Wi-Fi Alliance [4]), IEEE 802.11ad (TGad) [5], [6], IEEE 802.15.3c (TG3c) [7], Wireless HD (WiHD) [8], and Ecma International [9] have also accelerated this movement. Promising applications include uncompressed high-definition video transmission in homes [10], high-speed data transfer for PC applications, and high-speed file downloading.

To realize and disseminate such systems, two problems must be overcome. First, low-cost and low-power CMOS or SiGe-BiCMOS LSIs co-integrated with small steerable antennas must be developed in the millimeter-wave (MMW) frequency range, taking into account portable-equipment implementation and high-volume market development. Second, beamforming (BF) techniques or protocols must be established to combat degraded or disconnected communications links due to various channel variations and the unique propagation characteristics of MMWs.

For the first problem, 60-GHz band transceivers integrated with planar phased-array antennas (PAAs) have been developed based on CMOS [11] and SiGe BiCMOS [12] technologies in recent years thanks to rapid progress in Si LSI technologies [13]. Alternatively, for the second problem, various BF techniques have been proposed [14]–[24], some of which [14] have been adopted in the 60-GHz band standard specifications [25]. However, further investigations are still required, especially with considerations on actual MMW antenna characteristics. Experimental verifications using MMW transceiver LSIs with PAAs have rarely been reported, and hence are also in high demand.

Principal BF techniques adopted in the 60-GHz band standards are the "codebook-based protocol" [14] in TG3c [25] and the "iterative method" in WiGig [26]/TGad [27]. These techniques enable fast BF function under low hardware-complexity and low power-consumption constraints, by effectively utilizing the "quasi-omni-directional" antenna radiation pattern (Q-omni pattern). Here, Q-omni pattern is defined as a pseudo-isotropic radiation pattern having relatively constant antenna gain within a specific angle range. However, the Q-omni pattern with sufficiently small gain variation is usually difficult to be generated in actual MMW PAAs [28], and will be shown experimentally in this paper for the first time. In such cases, these techniques can miss the best link.

This paper proposes a BF technique, named Multiple sector-ID Capture (MIDC), which can precisely detect the best link under the imperfect Q-omni conditions. The BF technique proposed here also enables the ability to reserve multiple antenna setting pairs (ASPs) corresponding to existing communication links (wireless paths) in the order of their respective link qualities. This allows for fast beam switching

Manuscript received January 22, 2014; revised July 29, 2014; accepted October 15, 2014. Date of publication October 28, 2014; date of current version December 31, 2014.

K. Hosoya and S. Kishimoto are with the Green Platform Research Laboratories, NEC Corporation, Kawasaki 211-8666, Japan (e-mail: k-hosoya@ce.jp.nec.com).

N. Prasad and S. Rangarajan are with NEC Laboratories America, Princeton, NJ 08540 USA.

K. Ramachandran was with NEC Laboratories America, Princeton, NJ 08540 USA. He is now with Zipreel, Inc., North Brunswick, NJ 08550 USA.

N. Orihashi is with the Mobile Wireless Network Division, NEC Corporation, Kawasaki 211-8666, Japan.

K. Maruhashi is with the Smart Energy Research Laboratories, NEC Corporation, Kawasaki 211-8666, Japan.

Digital Object Identifier 10.1109/TAP.2014.2365209

when link blockage occurs in fixed-terminal (stationary-device) applications. The training is executed in short durations by putting together direction-of-arrival/direction-of-departure (DoA/DoD)-estimation and "beam combining (BC)" techniques. The basic function of MIDC is verified experimentally in a simple multipath propagation environment by using our 60-GHz CMOS transceiver LSIs with PAAs [11].

MIDC has been adopted in the MAC/PHY specifications of WiGig [26] and TGad [27] as an optional subphase supplementing the main BF phase based on the iterative method in [26], [27]. In a previous conference [28], the concept of MIDC was introduced very briefly. This paper describes MIDC in detail, along with analytical performance evaluations and experimental verifications.

The main contribution of this paper is the first proposal of BF protocol for 60-GHz band WLAN/PANs considering actual MMW PAA characteristics, along with the first experimental verification of it using one-chip MMW LSIs integrated with PAAs.

The rest of the paper is organized as follows. Section II discusses features of the 60-GHz propagation channel and the necessity of the BF function. Section III reviews related BF techniques proposed for 60-GHz band WLAN/PAN systems. Section IV shows the difficulty of Q-omni generation, which is a prime motive for this study. Section V describes MIDC in detail, while Section VI compares MIDC with the other BF protocols adopted in 60-GHz standards. Section VII demonstrates the results of experimental verification. Finally, Section VIII concludes this paper.

II. 60-GHz Propagation Channel and Need for BF Techniques

Characteristics of the 60-GHz propagation channel are quite different from those of the microwave (2.4 or 5 GHz) WLAN channel because of its short wavelength [29], [30]. It suffers from large path loss mainly due to high free-space propagation loss following Friis' equation [31]. While this enables spatial frequency reuse [32], high-gain directional transmission using antenna arrays is required [18] to compensate for the high attenuation and provide a sufficient link budget [12], [33]. Directional antennas incidentally bring benefits of interference mitigation [33], [34] and multipath suppression [33], [35]–[37]. The short wavelength also makes it possible to implement the antenna array in a small form factor.

On the other hand, because of "quasi-optical" [38] or "ray-like" nature (i.e., large penetration loss, and small diffraction), MMW signals tend to be obstructed by blockers such as human body [21] and various equipment, leading to serious degradation of link qualities. Besides BF, this link-blockage problem can be solved by system diversity [39] or multihop routing [10], [40]. However, system diversity and multihop routing incur system complexity and heavy signal processing or need other supporting hardware such as relaying devices [19]. This makes BF the ideal solution for the link-blockage problem in MMW systems, where the hardware should be kept simple and heavy signal processing should be avoided. This is the motivation for our work. We note that BF is also beneficial for neighbor discovery and resolving deafness/hidden-node problems [40] caused by the narrow half-power beamwidths of the MMW highly-directional antennas.

III. Related Work on BF Protocol for 60-GHz Band WLAN/PANs

To realize robust MMW systems over the aforementioned channel characteristics, various BF techniques have been reported for the 60-GHz band WLAN/PAN systems [32].

The "beam-codebook (training-matrix)-based protocol" [14] adopted in TG3c [25] and the "iterative method" in WiGig [26]/TGad [27] are important given that they have been adopted in the major 60-GHz standards. These two techniques will be reviewed and compared with MIDC in Section VI, because like MIDC they also rely on Q-omni patterns. On the other hand, a technique using the Hadamard matrix adopted in WiHD standard [8] is very robust, but requires heavy computational resources. Hence, it is not further discussed in this paper.

Multi-stage codebook design method [15] and DFT (discrete Fourier transform)-based codebook [16] have given more specific or robust implementation methods to the codebook-based protocol. On the other hand, several protocols similar to the iterative method using Q-omni have been proposed [16]–[18]. Since each of these works can be classified either as a codebook-based protocol and an iterative method, we focus our discussion on the original codebook-based protocol and iterative method.

A beam switching technique [19] was presented for the link blockage problems in 60-GHz WPANs. Since that technique is based on the backup-link concept, it is closely related to MIDC. However, it only provides how to select a link from the backup ones, but does not offer how to reserve the backup links, which is the main subject of MIDC.

A mathematical protocol to search the best beam pair using the Rosenbrock algorithm was also proposed [20]. It searches the best beam pair correctly since it does not use Q-omni, and is faster than the TG3c and TGad protocols especially for large-array sizes because this protocol follows a global optimization scheme. However, it does not have the function of the backup link generation.

MIDC applies DoA/DoD-estimation techniques along with the use of Q-omni for fast detection of beam candidates. Although the use of DoA/DoD-estimation for BF training in 60-GHz systems was mentioned [21], the approach differs from MIDC in the respect that it supposes only RX (receiver) training in point-to-multipoint scenarios and consequently does not use Q-omni.

DoA/DoD-estimation techniques have also been studied in 60-GHz band experimentally [37], [41], [42], and numerically [43]. These works however do not aim at applications with BF protocols.

Protocols [21]–[23] can be categorized as "digital BF [35]" (also known as "digital signal processing (DSP)-based BF [41]" or "element-space processing [34]"). This requires "digital BF array [21]" where a baseband digital processor or analog-to-digital/digital-to-analog converter (ADC/DAC) is present at each array element, and received signals from each array element are

processed and combined in the digital domain [24]. In wideband MMW systems, however, such architecture is difficult to implement owing to high power consumption, high cost of high-precision multi-Gbps ADC/DACs and the large number of array elements required to compensate for propagation loss [24], [41], [42]. Hence, MIDC is based on "analog BF [35]" (also called "beam-space processing [34]"), where received signals from each array elements are combined in the analog domain and then processed with only one processor.

IV. Difficulty of Good Q-omni Generation

Prior to describing MIDC, we must discuss the difficulty of Q-omni pattern generation with a sufficiently small gain variation by using steerable antennas such as PAAs or sector antennas in the MMW range. Although various BF techniques relying on Q-omni have been proposed for the MMW systems [14]–[18], [26], [27], they presuppose ideal Q-omni. This paper presents experimental Q-omni patterns of a MMW PAA for the first time and points out a problem in using it in BF protocols.

One reason for the difficulty of good Q-omni generation is that the antenna elements constituting the steerable antenna, electromagnetically affect each other. This makes it difficult to realize good Q-omni patterns even if the radiation pattern of the antenna element itself is sufficiently isotropic. Another reason is that the Q-omni pattern tends to be affected by the environment outside the antenna, such as enclosures on which the antenna is mounted, the radome of the antenna, and objects around the enclosures.

There are a few methods to generate the Q-omni pattern. The first is to activate multiple antenna elements and optimize the array weight vector (AWV) for minimizing gain variation in the required angle range. An advantage of this method is tolerance towards transmitter (TX)-receiver (RX) distance thanks to potentially high Q-omni gain for a limited angle range. However, it is generally difficult to obtain good Q-omni by this method, especially when AWV has very little freedom, for instance, when only the phases of the AWV components can be changed over a small finite set of values. Even when good Q-omni is predicted in theoretical optimization based on electromagnetic (EM) simulation or point-source approximation, emphasis of dips and protuberances is often observed in experiments. Fig. 1(a) shows an example of EM-optimized and measured Q-omni patterns generated by using a four-element linear PAA. The predicted (EM-simulated) gain variation of 8.2 dB in the range of $\pm 45^\circ$ was further increased to 15.6 dB in measurements due to the emphasis of dips and protuberances. One cause of this emphasis would be the manufacturing variation affecting the phase and amplitude of signals fed to (TX case) or received from (RX case) each antenna element.

The second method is to activate only one element. Relatively good Q-omni patterns can be obtained at the expense of slightly lower Q-omni gain[1] [Fig. 1(b)]. The measured gain variation is 7.7 dB in the range of $\pm 45^\circ$, while the simulated value is 3.8 dB.

[1]We selected an outside one because larger gain variation was observed when an inside element was activated. This would be attributed to the fact that the inside element is electromagnetically coupled with elements on both sides.

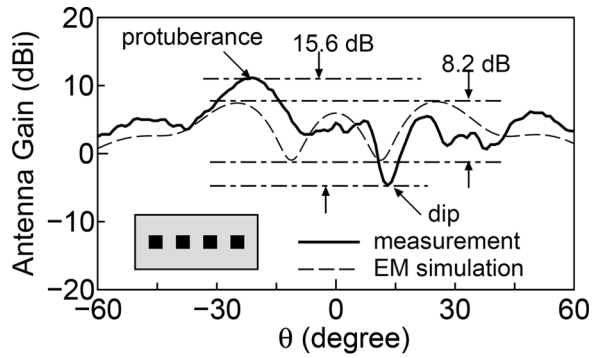

(a)

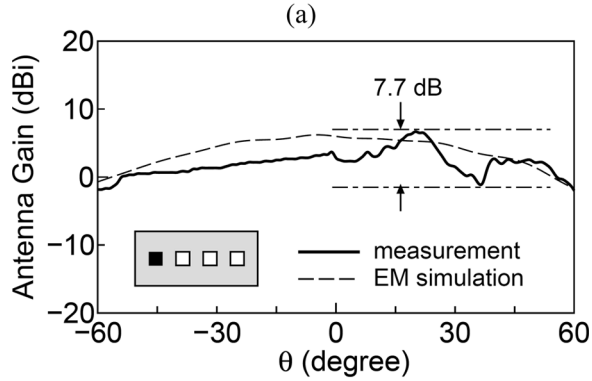

(b)

Fig. 1. Quasi-omni patterns of phased array antenna. (a) Using multiple elements (four element linear array). (b) Using one element. EM simulation curves were obtained by 3-D electromagnetic simulation (Ansoft HFSS [44]). The measurements were done by rotating a horn antenna around the evaluation board operating in the RX mode. Absolute values of measurement curves were calibrated by supposing that the measured antenna gain at the zenith of the zenith-directed beam agrees with simulated value.

The larger measured variation would be due to various EM effects from the evaluation board and the external environment.

The third method is to use an antenna specially prepared for Q-omni generation. This is impractical from the point view of the implementation area and hardware complexity, especially for mobile-instrument applications.

Since "good" Q-omni generation is very difficult in the MMW range as discussed above, we assert that the imperfection of Q-omni should be carefully considered if we use it in BF protocols. Among these three methods, we consider the second method as the best solution for indoor short-range communications such as WLAN/PANs and use it in Section VII of this work.

V. MIDC Protocol

A. Beam Reservation

The underlying concept of MIDC is "beam reservation." It means to reserve multiple ASPs corresponding to the links between the TX and RX in the initial BF training. Here, ASP means a pair of TX and RX AWVs for phased array antennas, sector IDs for sector antennas, and so on. Although the beam reservation is similar to the beam-switching [19] or backup-link concepts, this work puts emphasis on how to reserve backup ASPs. We therefore call it beam reservation in this paper.

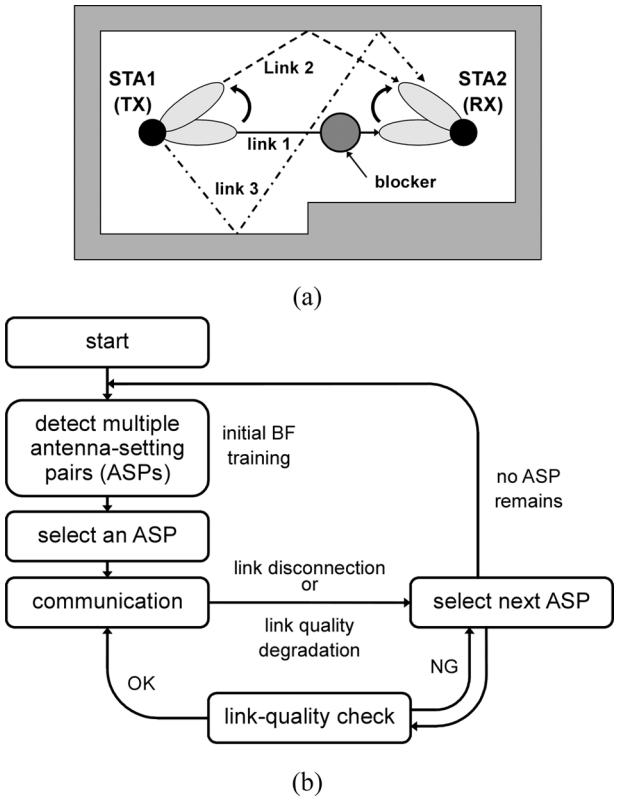

Fig. 2. Concept of "Beam Reservation." (a) Illustration of propagation environment (one-dimensional BF case). (b) Phase transition. ASPs can be reserved in memory arrays integrated in TRX LSI chips [12].

Consider a propagation environment in Fig. 2(a), with one line-of-sight (LOS) link (link 1) and two non-LOS (NLOS) links (links 2, 3). When the best link (link 1) is shut by a blocker, the TX and RX can immediately change their antenna setting to another one corresponding to the second-best link (link 2). An example of simplified phase transition is described in Fig. 2(b).[2]

The beam reservation presupposes the quasi-optical nature of MMWs (note that, in the microwave range, qualities of links other than the blocked one would also be affected by the blocker). This nature has been verified by agreement between ray-tracing and measurement results [17], [36], [38], [45]. In addition, it has been reported that reliable communication links can be established by using reflected signals of either the first order [19] or the first and second orders [32], [38] in 60-GHz indoor environments, which ensures validity of the reserved NLOS links.

Since the multiple ASPs are detected and reserved in the initial training, and not during communication, a relatively long duration is tolerated. For moving-device applications such as note PCs, however, the reserved ASPs become invalid when one of the devices moves, and thus the initial training must be done all over again. Similar situations occur when all the reserved links are blocked by multiple blockers (but usable links remain in the propagation environment). Accordingly, it is important to reduce the duration, even for protocols with the beam-reservation function.

[2]There might be a case where the LOS link is blocked during communication or initial training, and then the blocker is removed. For such a case, it is effective to keep probing channel status by carrying out the initial training during or in the intervals of communication, and constantly update the beam-reservation table. By doing so, the LOS link can be selected after next blockage if it is in the available state. A similar concept was mentioned in [19].

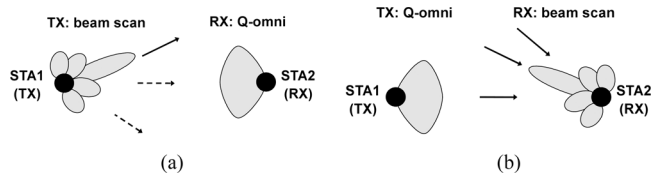

Fig. 3. Beam configurations in SLS/MID (DoD/DoA estimation). (a) SLS. (b) MID.

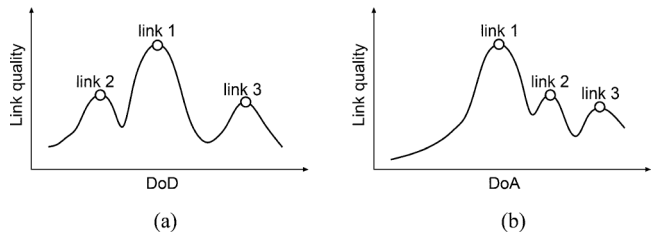

Fig. 4. Angle (link-quality versus DoD/DoA) profile. (a) SLS. (b) MID. For simplicity, a one-dimensional (1-D) BF case is described. In general 2-D BF cases, these profiles become contours on azimuth and elevation planes.

B. MIDC Procedure

1) SLS/MID (DoD/DoA Estimation): To realize the beam reservation in short duration, MIDC firstly executes DoD/DoA estimation by utilizing Q-omni. In this phase, the TX (or RX) beam is scanned by changing antenna settings ("beam-formed mode"), whereas the RX (or TX) beam on the other link end is kept in Q-omni mode, as illustrated in Fig. 3. In WiGig/TGad specifications, each process is called "sector level sweep (SLS) phase" and "multiple sector-ID detection (MID) subphase," respectively.

By performing SLS/MID, "angle profiles" representing the relationship between link quality [e.g., received power, signal-to-noise ratio (SNR) or bit error rate (BER)] and beam direction (DoD for SLS and DoA for MID) will be obtained as shown in Fig. 4. Some peaks (local maximum points) will be detected by an appropriate peak-search algorithm in directions where the links (propagation channels) exist.

From the profiles, numerical tables, named "beam candidates tables," such as those in Table I, are obtained. The antenna settings corresponding to the peaks in the angle profiles are listed in link-quality order. AWVs (as in this example), sector IDs, DoD/DoAs, or other quantities/indices can be used as antenna settings. When too many peaks exist, an upper limit on number of detected beams should be set to reduce the duration of the subsequent "beam combining (BC) subphase." Another way is to set a lower limit on link quality. In Table I, N_{beam}^{TX} peaks in SLS and N_{beam}^{RX} peaks in MID are detected.

2) Imperfect Quasi-Omni Problem: If the measurements in SLS/MID are perfectly accurate, it is enough to combine TX and RX antenna settings in the same order, e.g., AWV(TX, i) and AWV(RX, i) ($i = 1, 2, \ldots$) in Table I. In practice however, there exist various error factors in the profile. Especially when there are links with similar path loss, these error factors may induce various problems if the above-mentioned straightforward

TABLE I
BEAM CANDIDATES TABLES OBTAINED IN SLS/MID

order of link quality	antenna setting
1	AWV (TX, 1)
2	AWV (TX, 2)
⋮	⋮
N_{beam}^{TX}	AWV (TX, N_{beam}^{TX})

order of link quality	antenna setting
1	AWV (RX, 1)
2	AWV (RX, 2)
⋮	⋮
N_{beam}^{RX}	AWV (RX, N_{beam}^{RX})

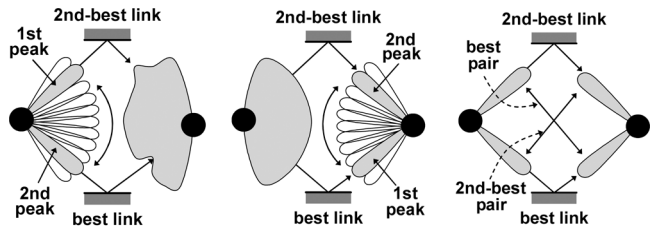

Fig. 5. Effect of quasi-omni imperfection (wrong pairing). (a) SLS. (b) MID. (c) Pairing.

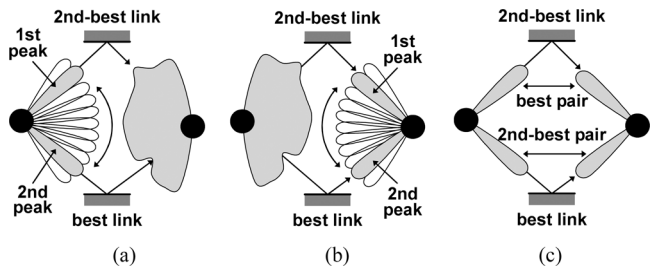

Fig. 6. Effect of quasi-omni imperfection (wrong pair order). (a) SLS. (b) MID. (c) Pairing.

pairing method is applied. The error factor to be specially considered is the imperfection in Q-omni used in SLS/MID, discussed in Section IV.

Let us consider a simple case where two links (best and second-best link) exist. If SLS and/or MID is executed by using imperfect Q-omni, and the straightforward pairing is applied, a problem illustrated in Fig. 5 would occur. Peak levels corresponding to each link in the SLS profile may be reversed to an incorrect order, leading to "wrong pairs" of antenna settings in pairing. Here, a "wrong pair" is defined as a combination of TX and RX antenna settings whose mainlobes are not directed to the same propagation link. Since link quality for such wrong pairs would usually be very poor, such pairing errors must be avoided.

Even if pairing is carried out correctly, the order of pairs can differ from the link-quality order (Fig. 6). Such an error should also be avoided because the ASP regarded as the best (in fact, corresponding to the second-best link) is used in communication with first priority.

3) Beam Combining (BC): To resolve these problems, MIDC executes a round-robin trial between the detected beam candidates of the TX and RX in the BC subphase. Beam configurations and conceptual diagram are illustrated in Fig. 7. Since the number of beam candidates is extremely reduced

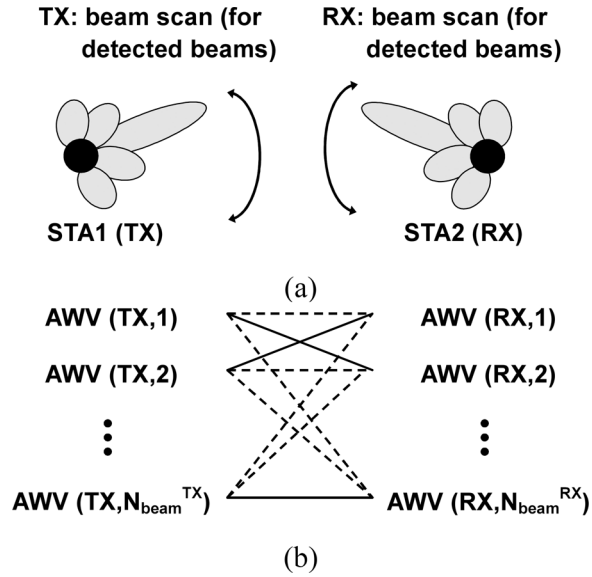

Fig. 7. Beam combining (BC). (a) Beam configuration. (b) Conceptual diagram. Although this process can be also called as "beam pairing," we use the term "beam combining" in this paper in accordance with the WiGig/TGad specifications [26], [27].

TABLE II
BEAM RESERVATION TABLE OBTAINED IN BC

order of link quality	antenna setting pair (ASP)	
	STA1 (TX mode)	STA2 (RX mode)
1	AWV (TX, 1)	AWV (RX, 3)
2	AWV (TX, 2)	AWV (RX, 1)
⋮	⋮	⋮
N_{beam}	AWV (TX, i)	AWV (RX, j)
⋮	⋮	⋮
$N_{beam}^{TX} \times N_{beam}^{RX}$	AWV (TX, k)	AWV (RX, l)

through SLS/MID, this round-robin trial does not considerably increase the training duration. As a result of BC, a list of ASPs, named "beam reservation table," such as Table II is obtained. Note that each TX AWV appears multiple ($N_{\rm beam}^{RX}$) times in the STA1 (station 1) column, and vice versa. Since most of the $N_{\rm beam}^{TX} \times N_{\rm beam}^{RX}$ combinations are "wrong" pairs, only a small number ($N_{\rm beam}$ above the double line in Table II) of pairs at higher ranks should be reserved for data communication. The number, $N_{\rm beam}$, should be a predetermined number (for example, $N_{\rm beam} = \min(N_{\rm beam}^{TX}, N_{\rm beam}^{RX})$ is a reasonable choice), or determined by a lower limit on link quality.

The BC subphase uses only beams in the beam-formed mode, which will be utilized in actual data communication. In other words, Q-omni is not used. This substantially ensures the correct combination of antenna settings in right order.

Note that the effect of imperfect Q-omni can not be completely eliminated even by MIDC. Some of the AWVs corresponding to upper $N_{\rm beam}$ links can be left out of Table I. Hence Q-omni gain must be isotropic to some extent even in MIDC.

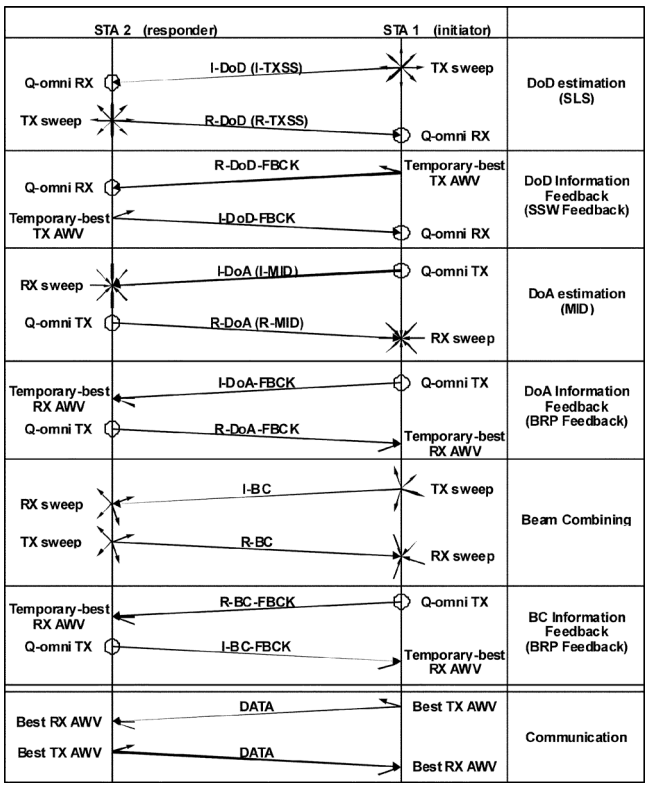

Fig. 8. Basic diagram of MIDC. "I," "R," and "FBCK" are abbreviations for "initiator," "responder," and "feedback," respectively. Terms in parentheses indicate those in WiGig/TGad specifications.

4) Communication: After the initial training, data communication should be started using the best ASP. When a link quality degradation or disconnection is detected, the TX and RX change their antenna settings to the second-best one. After link-quality check (if needed), data communication is resumed [see Fig. 2(b)]. Here we suppose that the link quality of the second-best link is preserved when the best link is shut by a blocker, owing to the quasi-optical nature of MMWs. This viewpoint will be verified experimentally in Section VII.

C. Diagram

The basic diagram of MIDC for both link directions (STA1 to STA2, and vice versa) is shown in Fig. 8. In "sector sweep (SSW) feedback" and "beam refinement protocol (BRP) Feedback," a lot of information is exchanged between STAs. In "R-DoD-FBCK," for example, "R-DoD" results in SLS (detected antenna settings or measured data) are fed back from STA1 to STA2. Details are mentioned in [26], [27]. "Beam refinement transaction" (BRT hereafter) may be executed as necessary between "BC information feedback" and "communication," where the antenna settings are tuned in an iterative manner [26], [27].

Note that the term "MIDC" is defined as a subphase including the MID and BC subphases in WiGig/TGad specifications. Our primary contribution to WiGig/TGad specifications is the introduction of these MID and BC subphases, whereas we leverage SLS phase present in the specifications.

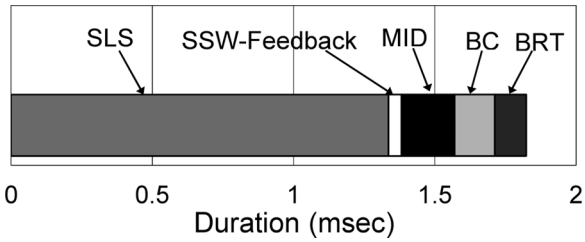

Fig. 9. Calculated duration of MIDC (typical). Following parameters were used: number of antenna settings in SLS $= 32$, number of antenna settings in BRT $= 32$, $N_{\mathrm{beam}}^{TX} = N_{\mathrm{beam}}^{RX} = 7$, number of iterations for BRT is 2, and SBIFS $= 0.73$ (μs).

D. BF Duration

This section describes how the BF duration (the initial BF training setup time) of MIDC is estimated. Primary parameters are listed in caption of Fig. 9. Other parameters are in accordance with WiGig/TGad specifications [26], [27]. BRT, not included in Fig. 8, is added after the MIDC procedure according to WiGig/TGad specifications.

Calculated result (Fig. 9) shows that BC has little effect on total duration in spite of its round-robin trial. On the other hand, SLS is a dominant factor. This is because "Control PHY packet" is used in SLS, where one preamble must be transmitted per one antenna setting. The whole duration is about 1.8 ms. This value is greater than 1 ms, which is the limit on tolerable duration for uncompressed video streaming [46] due to finite transmitter and receiver buffer sizes. However, it is acceptable due to the following reasons: (1) MIDC is basically the initial training before starting communication. Even when a link is blocked, the beam will switch immediately and the MIDC procedure will not repeat. (2) When a station moves, the whole MIDC procedure must be re-executed. Such a situation rarely occurs in cases where the BF-duration requirement is very strict, e.g., uncompressed video streaming between TVs and DVD players.

E. Sidelobe Problems

Since MIDC applies DoA-estimation techniques to multipath environments, it would inherently suffer from sidelobes of steerable antennas. If DSP-based methods [47], such as Capon, linear-estimation, minimum-norm, multiple signal classification (MUSIC), or estimation of signal parameters via rotation invariance techniques (ESPRIT) methods, can be used, the sidelobe effects would be sufficiently suppressed. In MMW range, however, such methods are difficult to implement as discussed in Section III. This obliges us to use simple methods without sophisticated signal processing, such as the beamformer method [47], which are directly affected by the sidelobes.

The problems are caused by strong multipath signals that are radiated from (SLS case) or received by (MID case) high-level sidelobes. These multipath signals produce errors which are shown in the values on the vertical axis in the profile, since a value on the vertical axis at a DoD/DoA is not purely due to a single signal radiated to or received from the DoD/DoA direction, but due to multipath signals radiated to or received from multiple directions. Accordingly, the following deteriorations of the profile can be induced.

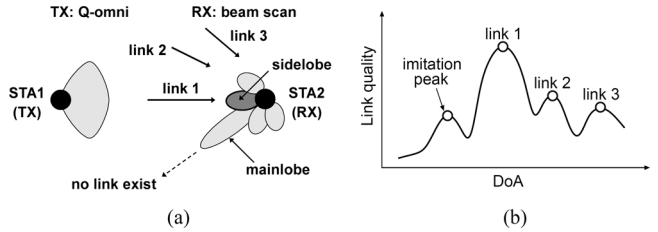

Fig. 10. 'Imitation peak" phenomenon. (a) Beam configuration. (b) Angle profile.

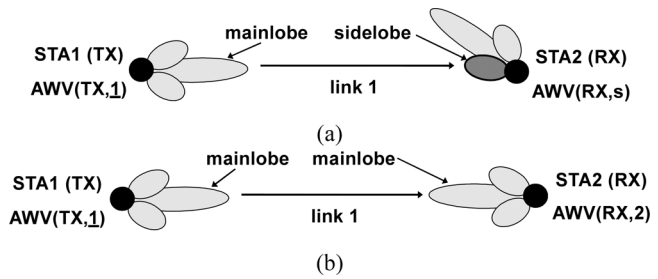

Fig. 11. Beam configurations for sidelobe-related and normal pairs. (a) Sidelobe-related pair. (b) Normal pair using the same link.

1) Imitation Peak: The most important deterioration phenomenon is the appearance of an "imitation peak" in the profile. Fig. 10(a) illustrates an example of this situation in MID. In this situation, RX turns its mainlobe to a direction where there is no link, while the direction of a sidelobe is consistent with the best (LOS) link. In such a case, the strong signal is detected by the sidelobe. As a result, the leftmost peak can appear in the profile of Fig. 10(b) at DoA corresponding to the mainlobe of Fig. 10(a). This peak is due to the sidelobe, and so does not represent a real link direction. Therefore, we call this kind of peak as "imitation peak" hereafter. The same phenomena would occur in SLS too.

Next, let us consider the effects of the imitation peaks. If the imitation peak is detected in MID for example, a pair including an antenna setting corresponding to the imitation peak may appear at a high rank in the beam-reservation table (nth order in Table III). The beam configuration in BC for the sidelobe-related pair is illustrated in Fig. 11(a). It is worth noting that this beam configuration can be used for communication if it has enough link quality. However, it should be remembered at the same time that a pair whose mainlobes are directed toward the same link [Fig. 11(b)] surely exists at a higher rank (e.g., the first order in Table III). If the pair (b) becomes unusable by a blocker, the pair (a) is also out of use because the same link is used in both the pairs. Hence the pair (a) is of low value as a reserved one and should be excluded from the reservation table (or its rank should be lowered).

To exclude the sidelobe-related pair, we must discern such a pair from the others. However, we cannot distinguish an imitation peak simply from the profile (SLS/MID results). In Table III (BC results), on the other hand, we can see that the same antenna setting, AWV(TX, 1), appears multiple (two) times at high ranks (the first and the nth orders, both of which are within N_{beam}) in the STA1 antenna setting column. It suggests that AWV(RX, s), the antenna setting of the opposite STA, is the one using sidelobe. Hence, we should exclude the nth-order pair from the table. By applying this simple rule, we can exclude the sidelobe-related pair from the reservation table.

TABLE III
BEAM RESERVATION TABLE INCLUDING SIDELOBE-RELATED PAIR

order of link quality	antenna setting pair (ASP)	
	STA1 (TX mode)	STA2 (RX mode)
1	AWV (TX, 1)	AWV (RX, 3)
2	AWV (TX, 2)	AWV (RX, 1)
⋮	⋮	⋮
n	AWV (TX, 1)	AWV (RX, s)
⋮	⋮	⋮
N_{beam}	AWV (TX, i)	AWV (RX, j)
⋮	⋮	⋮
$N_{beam}^{TX} \times N_{beam}^{RX}$	AWV (TX, k)	AWV (RX, l)

2) Blunting of Profile: Another sidelobe-induced phenomenon is a blunting of the profile [48], which may not only produce errors in both link-quality and DoA/DoD values, but in a worse case, make it difficult to detect the second and following peaks. We can cope with this problem without the use of DSP-based algorithms, for example, by a fixed-null sweep technique [48] although we have not detailed it in this paper.

VI. COMPARISON WITH OTHER PROTOCOLS IN 60-GHz BAND STANDARDS

This section compares MIDC with the two conventional protocols adopted in the 60-GHz band standards: the codebook-based protocol [14], [25] in TG3c and the iterative method [26], [27] in WiGig/TGad, both of which utilize Q-omni pattern as does MIDC. The comparison is done from two points of view: tolerance to Q-omni imperfection and BF duration.

A. Conventional Protocols

1) Codebook Based Protocol: This protocol [14] uses three kinds of beams with different angle resolutions (beam width). They are named "Q-omni pattern," "sector," and "beam," and range from wide to narrow beam order. First, a round-robin trial between TX and RX Q-omni patterns is executed ("Q-omni pattern training"). Following that is a round-robin trial between TX and RX sectors included in the best Q-omni patterns identified in the Q-omni pattern training ("sector-level searching"). Finally, beams included in the selected sectors are tested in the round-robin manner ("beam-level searching"). By dividing the test stages, the number of combinations tested can be substantially reduced as compared to the case where exhaustive full round-robin trial of beams is executed.

2) Iterative Method: A typical scenario of this method [26], [27] is as follows. It also uses beam patterns with different resolutions. The coarse pattern is called "sector" while the fine pattern is called "beam." First, the best sector is determined temporarily by carrying out the SLS. Then the iterative procedure

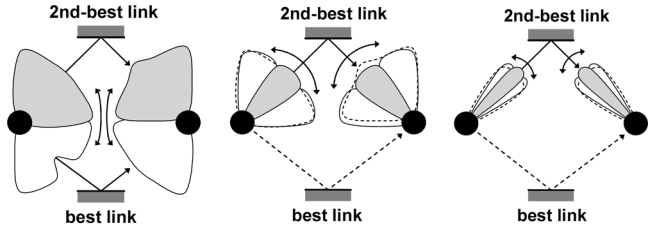

Fig. 12. Beam-codebook based (IEEE 802.15.3c) protocol [14], [25] under imperfect quasi-omni effect. (a) Quasi-omni pattern training. (b) Sector-level searching. (c) Beam-level searching.

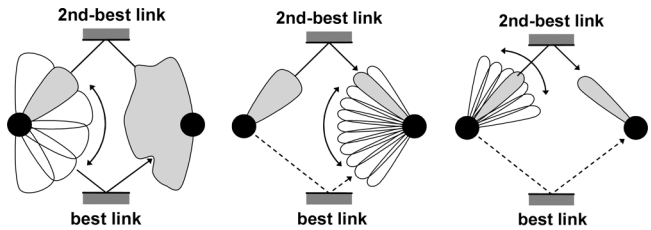

Fig. 13. Iterative (WiGig, IEEE802.11ad) method [26], [27] under imperfect quasi-omni effect. (a) SLS. (b) BRT1. (c) BRT2.

(BRT) follows. Here, RX beam is scanned while the TX pattern is fixed at the sector determined by the SLS. Next, TX beam is scanned while RX pattern is maintained at the best beam in the previous stage. Similar procedures are repeated for a pre-determined number of times. By determining the best sector of one STA initially, a full round-robin trial is avoided.

B. Tolerance to Q-omni Imperfection

This means ability to precisely detect the best link under imperfect Q-omni conditions. This subsection discusses this aspect by 1) qualitative, 2) analytical, and 3) numerical approaches.

1) Qualitative Consideration: In the codebook-based protocol, a problem may occur if the Q-omni pattern is imperfect. Consider a case where the best and second-best links exist. If the Q-omni pattern has a dip at the best link direction and/or a protuberance at the second-best link direction, the Q-omni patterns corresponding to the second-best link may be selected as shown in Fig. 12(a). Accordingly, the best link is never discovered in the following sector and beam-level searching stages [Figs. 12(b) and 12(c)].

In the iterative method, a similar problem can occur if the Q-omni pattern used in SLS is not perfect. Due to dips and/or protuberances in Q-omni, the sector directed to the second-best link may be selected in the SLS as illustrated in Fig. 13(a). Once the wrong sector is selected first, the best beam pair would never be detected no matter how many times the iterative procedures are repeated [Figs. 13(b) and 13(c)].

In MIDC, on the other hand, these problems are avoided by executing the BC subphase as discussed in Section V-B.

2) Analytical Evaluation: Probability of the above-discussed error (i.e., the probability of missing the best link) for the codebook-based, iterative, and MIDC protocols under the imperfect Q-omni condition is analytically evaluated here.

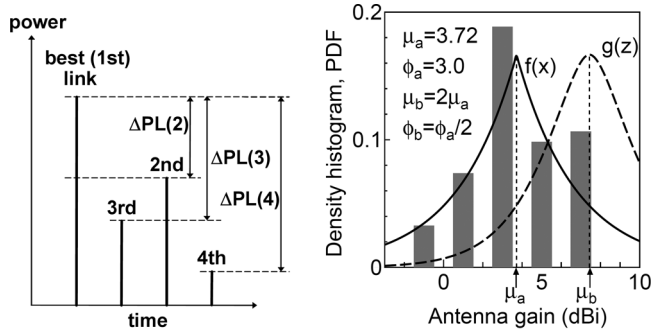

Fig. 14. Model for error probability estimation. (a) Channel model (delay profile). (b) Q-omni gain fluctuation model. This example histogram was obtained from EM simulation curve in Fig. 1(a).

A simple channel model is supposed as illustrated in Fig. 14(a). Path losses (in dB) of ith link ($i = 2, 3, \ldots, N_{\text{link}}$) can be written as

$$PL(i) = PL(1) + \Delta PL(i) \tag{1}$$

where $PL(1)$ denotes the path loss of the best link (link-1) and N_{link} is the number of the links.

Here we assume that DoA/DoD of each link can be considered as an independent random variable having the uniform distribution. As a result, Q-omni gain for each link also becomes a random variable via the relation shown in Fig. 1. If we convert a random variable from DoA/DoD to the Q-omni gain (X in dBi), its probability density function (pdf) can be approximately estimated by fitting the Q-omni gain histogram shown in Fig. 14(b). Based on EM simulations on various Q-omni patterns, we adopt the Laplace distribution[3]

$$f(x) = \frac{1}{2\phi_a} \exp\left(-\frac{|x - \mu_a|}{\phi_a}\right) \tag{2}$$

as shown by the solid line in Fig. 14(b).[4]

Let $G_L(i) = X(i) - PL(i)$ be the link gain for the ith link ($i = 1, 2, \ldots, N_{\text{link}}$) and E_i denote the event that $G_L(1) > G_L(i) (i = 2, \ldots, N_{\text{link}})$. Here, the random variable $X(i)$, $i = 1, 2, \ldots, N_{\text{link}}$, denotes the Q-omni gain of the ith link, and these variables are mutually independent.

For the iterative method and MIDC, if the Q-omni gain for the ith link does not exceed that for the best link by more than $\Delta PL(i)$, the link-gain order of these links does not reverse. When $X(1)$ is fixed to x_1, its probability is given by the cumulative distribution function (cdf)

$$F(x_1 + \Delta PL(i)) \equiv \int_{-\infty}^{x_1 + \Delta PL(i)} f(x)dx. \tag{3}$$

[3]The Laplace distribution was selected because 1) it can approximately represent the Q-omni gain fluctuations, and 2) it can be analytically integrated. We note that a truncated Laplace distribution can instead be used for better modeling but at the expense of analytical tractability.

[4]The initial values for the parameters μ_a and ϕ_a were estimated by using the maximum likelihood method, but then adjusted by giving weight to the region where the data are available.

In the iterative method, the reversal between the best link and any of the second and succeeding links leads to the error. Hence, the error probability can be written as

$$P_{err}^{ite} = 1 - P_r(E_2 \cap E_3 \cap \cdots \cap E_{N_{\rm link}}) = 1 - \int_{-\infty}^{\infty} f(x_1) \prod_{i=2}^{N_{\rm link}} F(x_1 + \Delta PL(i))dx_1 \quad (4)$$

where $P_r(\cdot)$ denotes the probability. On deriving (4), it should be noted that the events $E_i (i = 2, \ldots, N_{\rm link})$ are not mutually independent since they all involve common random variable $X(1)$. Hence, $P_r(E_2 \cap E_3 \cap \cdots \cap E_{N_{\rm link}}) \neq \prod_{i=2}^{N_{\rm link}} P_r(E_i)$.

Meanwhile, in MIDC, it is enough that the link-1 is selected as upper $N_{\rm beam}$ links at both the TX and RX, because the upper $N_{\rm beam}$ antenna settings are tested without using Q-omni in the succeeding BC subphase. Here, we assumed $N_{\rm beam}^{TX} = N_{\rm beam}^{RX} = N_{\rm beam}$ for simplicity. In other words, the reversals between the best link and no more than $(N_{\rm beam} - 1)$ links are allowed. In this case, the error probability can be written as

$$P_{err}^{MIDC} = 1 - \left[\overline{P}_{err}^{ite} + \sum_{r=1}^{N_{\rm beam}-1} \left\{ \sum_{\rm subset} \int_{-\infty}^{\infty} f(x_1) h(x_1) dx_1 \right\} \right]^2 \quad (5)$$

where

$$h(x_1) \equiv \prod_{j=1}^{r} \overline{F}(x_1 + \Delta PL(i_j)) \cdot \prod_{k=r+1}^{N_{\rm link}-1} F(x_1 + \Delta PL(i_k)) \quad (6)$$

and $\overline{P}_{err}^{ite} \equiv 1 - P_{err}^{ite}$, $\overline{F}(x) \equiv 1 - F(x)$. $\sum_{\rm subset}$ denotes the sum for all subsets $\{i_1, i_2, \ldots, i_r\} \subset \{2, 3, \ldots, N_{\rm link}\}$, while $\{i_{r+1}, i_{r+2}, \ldots, i_{N_{\rm link}-1}\}$ denotes their complementary sets. The square operation comes from the fact that the link-1 must be selected as upper $N_{\rm beam}$ links at both the TX and RX in MIDC case. The second term in the square brackets in (5) represents the improvement factor due to MIDC. It is apparent that this factor increases with increasing $N_{\rm beam}$ because the terms in the curly brackets have positive values.

On the other hand, in the "Q-omni pattern training stage" of the codebook-based protocol, the training signal is affected by the Q-omni fluctuation twice (TX/RX). If we consider the random variables X_t, X_r (TX and RX Q-omni gain) as independent and identically distributed, the pdf for $Z \equiv X_t + X_r$ is given by

$$g(z) = f * f = \int_{-\infty}^{\infty} f(x) f(z - x) dx. \quad (7)$$

The Q-omni patterns in this protocol are ones that divide the Q-omni patterns in the iterative method and MIDC into smaller pieces, and consequently each such pattern covers only a part of the whole angle range [see Fig. 12(a)]. This leads to smaller gain fluctuations. Hence, although the pdf for each antenna gain is given by (2), ϕ_a should be replaced by one with a smaller value, ϕ_b ($\phi_b < \phi_a$). Substituting (2) with $\phi_a \to \phi_b$ into (7) yields

$$g(z) = \frac{1}{4\phi_b} \exp\left(-\frac{|z - \mu_b|}{\phi_b}\right) + \frac{|z - \mu_b|}{4\phi_b^2} \exp\left(-\frac{|z - \mu_b|}{\phi_b}\right) \quad (8)$$

where $\mu_b = 2\mu_a$. Here we assume that the Q-omni gain fluctuation is halved in dBi by dividing Q-omni ($\phi_b = \phi_a/2$) as plotted by the dashed line in Fig. 14(b).

Since the sectors and beams are divided into fully narrow angles [see Figs. 12(b) and 12(c)] and have small gain fluctuations in the "sector-level searching" and "beam-level searching" stages, we can ignore the effects of these stages. Under such an assumption, the error probability for the codebook-based protocol is approximately given by

$$P_{err}^{CB} \simeq 1 - \int_{-\infty}^{\infty} g(z_1) \prod_{i=2}^{N_{\rm link}} G(z_1 + \Delta PL(i)) dz_1 \quad (9)$$

analogous to (4), where $G(z)$ denotes the cdf of Z.

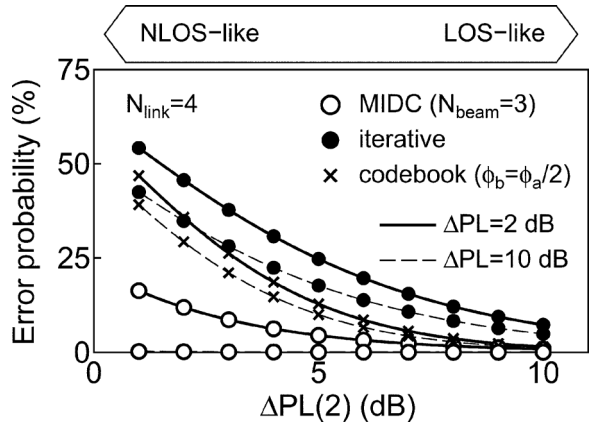

Fig. 15. Error probabilities based on analytical model (4), (5), and (9).

Fig. 15 compares the error probabilities for the three protocols based on (4), (5), and (9). Here we suppose $\Delta PL(i) = \Delta PL(i-1) + \Delta PL$ (dB) for $i = 3, \ldots, N_{\rm link}$ ($N_{\rm link} = 4$), and varied $\Delta PL(2)$ as a variable from 1 to 10 dB and ΔPL as a parameter from 2 to 10 dB to cover a wide range of 60-GHz band indoor channel models [45], [49]. Large $\Delta PL(2)$ represents LOS-like propagation environment, whereas small $\Delta PL(2)$ NLOS-like one.

In the iterative method and codebook-based protocol, the error probability rapidly increases with decreasing $\Delta PL(2)$ (NLOS-like scenario), while it remains low in MIDC.

The error probability of the codebook-based protocol improves rapidly with increasing $\Delta PL(2)$ and approaches that of MIDC. This can be attributed to the fact that $g(z)$ approaches zero rapidly when z departs from μ_b.

3) Numerical Verification: The above analytical model of the error probability is verified numerically for the iterative method and MIDC. We suppose the situation that signals from $N_{\rm link}$ links are detected by an imperfect Q-omni pattern in SLS. Path loss of each link is given by the channel model shown in Fig. 14(a). DoAs of each link are randomly determined 1000 times based on the uniform random distribution. The Q-omni

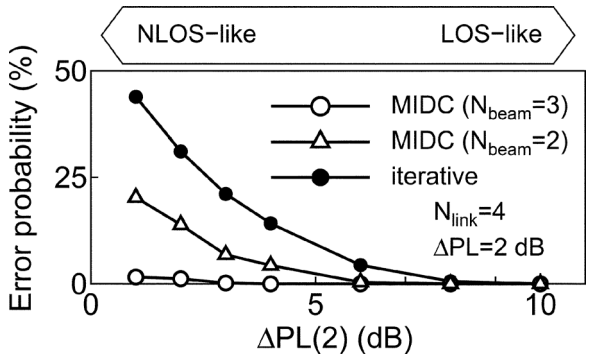

Fig. 16. Error probabilities based on numerical method ($N_{\rm link} = 4$, $N_{\rm beam} = 2,\ 3$, and $\Delta PL = 2$ dB). Note that this result is for a simple implementation of the iterative method. Other implementations can yield different performance.

gain for each link (each DoA) is then calculated by using the Q-omni pattern such as Fig. 1(a). The relative received power (link gain) can be calculated for each link and for each 1000-times trial from the above-obtained path loss and Q-omni gain values.

For the iterative method, the error probability can be defined as the probability that the real best link (link-1) does not receive maximum power and consequently is not selected as the best link. Meanwhile in MIDC case, it is defined as the probability that the link-1 is not selected as upper $N_{\rm beam}$ links at the TX and/or RX.

As shown in Fig. 16, the error probability is well suppressed by using MIDC ($N_{\rm beam} = 3$). For reference, a result for MIDC with $N_{\rm beam} = 2$ is also plotted. The error probability of MIDC is not sufficiently suppressed in this case on account of small $N_{\rm beam}$ as compared to the $N_{\rm beam} = 3$ case. These results not only demonstrate effectiveness of MIDC, but also give a guideline for selecting $N_{\rm beam}$.

C. BF Duration

Next, the BF duration is compared. However, direct comparison of BF duration among different specifications is difficult or unfair. It is because different MAC/PHY parameters are used in each specification and each protocol might be optimized for these parameters. Hence, we use the required number of measurements as an indicator of BF duration. We assume the following:

1) Angle range to be searched is common for three protocols.
2) The range is covered by a single Q-omni pattern in the iterative method and in MIDC.
3) Final beam resolution is also common.
4) No BRT iteration for MIDC.
5) Minimum (two iterations of) BRT for the iterative method.
6) DoA/DoD estimation in MIDC is done with the final beam resolution (resolution of "beam" in the codebook-based and iterative protocols).
7) SLS in the iterative method is done with a resolution same as "sector" in the codebook-based protocol, while BRT is with final resolution ("beam").

Let us represent the number of Q-omni, sectors, and beams in the codebook-based protocol as n_q, n_s, n_b, respectively, and let $N \equiv n_q \times n_s \times n_b$. From the above assumptions, beam configurations for the three protocols can be illustrated as in Fig. 17. According to the figure, the required number of measurements for one link direction (STA1 $\rightarrow$ STA2) can be estimated as in "simplified" case of Table IV, with an assumption $\gamma = 1$ in Fig. 17 for simplification. "Further simplified" case in the table represents the case where one more assumption $n_q = n_s = n_b$ is introduced as in [14]. Even if ${N_{\rm beam}}^2$ is ignored, $3{n_q}^2 < 2{n_q}^3$ holds when $n_q > 1.5$, which is usually satisfied. It means that the codebook-based protocol is faster than MIDC under the assumptions above. On the other hand, comparison between MIDC and the iterative method depends on the value of ${N_{\rm beam}}^2$ (number of beams in BC) and ${n_q}^2$ (number of sectors in SLS). It largely depends on the resolution of SLS. In the "example" of Table IV, typical measurement numbers are shown for a case of $n_q = n_s = n_b = 4$ [14] and $N_{\rm beam} = 7$. The duration of MIDC is expected to be about thrice as long as that of the codebook-based protocol and on the same level as that of the iterative method if all protocols are implemented in the same specification.

Of course, the duration depends on not only the number of measurements but also the kind of packets, IFSs (inter-frame separations), and so on. However, the above result is a good indicator of the BF-duration comparison among different specifications.

D. Summary of Comparison

Table V compares three protocols from three viewpoints. Advantages of MIDC are the ability to precisely detect the best link under imperfect Q-omni conditions and the beam-reservation function. BF duration is somewhat longer than that for the codebook-based protocol. However, since there is no need to repeat the initial training procedure when link blockage occurs in stationary-device applications, MIDC is not inferior to the codebook-based protocol even in terms of BF duration. This comparison suggests that MIDC is a strong candidate for BF protocol at MMW range. These protocols should be selectively adopted according to the use case (required angle range, possibility of STA movement etc.) and transceiver performance (Q-omni characteristics, sidelobe levels, etc.). For future study, more exhaustive simulations are required both on the tolerance to Q-omni and the BF duration based on more detailed channel model [49] and PHY-related parameters [14].

VII. Experimental Verification

Although various BF protocols have been proposed for 60-GHz WLAN/PAN systems as reviewed in Section III, most of the verification studies have been based on simulations [18], [21], and experimental verification has rarely been reported. Celik [22], [23] presented adaptive BF experiments based on his hybrid algorithm, but used a prototype hardware composed of multiple MMICs, external signal source, and horn-antenna array, rather than a one-chip LSI integrated with planar PAA that will be used in real communication systems.

In contrast, we present preliminary experiments using one-chip LSI with PAA for verification of MIDC. In our experiments, AWVs were controlled by manual operation, not by automatic one, because we focused on issues related to MMW prop-

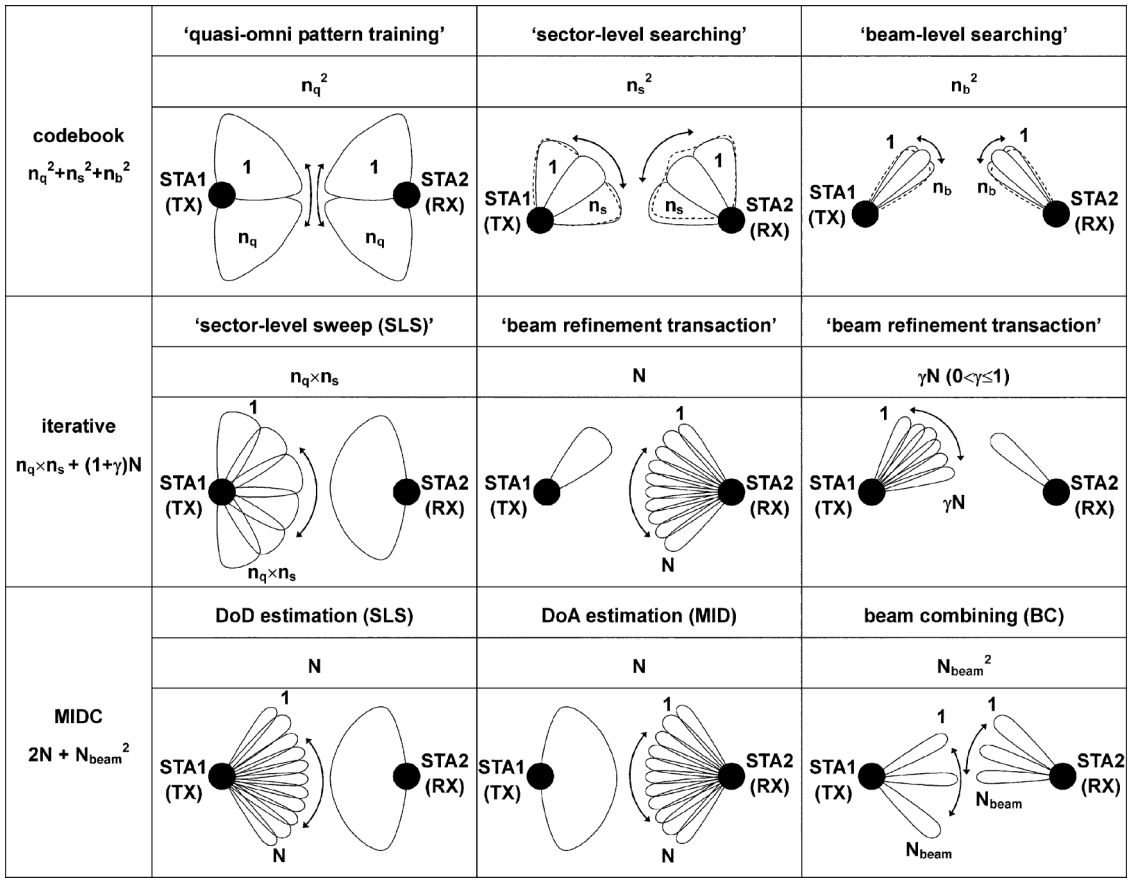

Fig. 17. Duration (number of measurements) comparison of BF protocols for 60-GHz band WLAN/PANs: codebook-based protocol [14], [25], iterative method [26], [27], and MIDC. Number of measurements is counted for only one-direction link (from STA1 to STA2). A coefficient γ $(0 < \gamma \leq 1)$ is added in the second BRT (beam refinement transaction) of iterative method because the second BRT is executed only around previous best sector direction. For simplicity, we assume $N_{\mathrm{beam}}^{TX} = N_{\mathrm{beam}}^{RX} = N_{\mathrm{beam}}$.

TABLE IV
REQUIRED NUMBER OF MEASUREMENTS FOR 60-GHz BAND WLAN/PAN BF PROTOCOLS, CODEBOOK-BASED PROTOCOL [14], [25], ITERATIVE METHOD [26], [27], AND MIDC

	simplified	further simplified	example
codebook	${n_q}^2 + {n_s}^2 + {n_b}^2$	$3{n_q}^2$	48
iterative	$n_q \times n_s + 2N$	${n_q}^2 + 2{n_q}^3$	144
MIDC	$2N + {N_{beam}}^2$	$2{n_q}^3 + {N_{beam}}^2$	177

TABLE V
COMPARISON OF BF PROTOCOLS FOR 60-GHz BAND WLAN/PANS, CODEBOOK-BASED PROTOCOL [14], [25], ITERATIVE METHOD [26], [27], AND MIDC

	codebook	iterative	MIDC
BF duration (number of meas.)	very fast	fast	fast
tolerance to Q-omni	average	average	high
beam-reservation function	no	no	yes

agation characteristics: (1) can we get the angle profiles and detect peaks, (2) will the sidelobe problems appear and can we cope with them, and (3) will link quality be preserved when another link is blocked.

A. MMW Transceivers

We used transceivers (TRX) integrating CMOS LSIs and planar PAAs developed by our group. The CMOS LSI is based on standard 90-nm technology and includes eight TX and RX frontends. Each frontend basically has the same architecture and circuits as in [11] except for some minor modifications. The PAA also has a similar structure as in [11], but has 2×4 elements for each TX and RX, respectively. Each element is a square patch antenna placed at a spacing of 0.75λ.

In this work, 1-D BF was carried out for simplicity. Hence, only 1×4 of 2×4 elements were used in the beam-formed modes. The phase of signal fed to (or received from) each antenna element was controlled in $\pi/2$ steps by 2-bit baseband phase shifters integrated in the LSI [11]. Signal amplitude was not controlled. Therefore, the AWVs in this study can be written as $\boldsymbol{w} \equiv [e^{j\varphi_1}, e^{j\varphi_2}, e^{j\varphi_3}, e^{j\varphi_4}]^T$, where $j = \sqrt{-1}$ and each phase φ_k $(k = 1$ to $4)$ takes any value from among 0, $\pi/2$, π, and $3\pi/2$. For the Q-omni mode in SLS/MID phase, only one element was activated to ensure small gain variation (see Fig. 1).

B. Antenna Radiation Pattern

Along with Q-omni, antenna radiation patterns in the beam-formed modes, especially its sidelobes, have serious effects on MIDC performance as discussed in Section V.

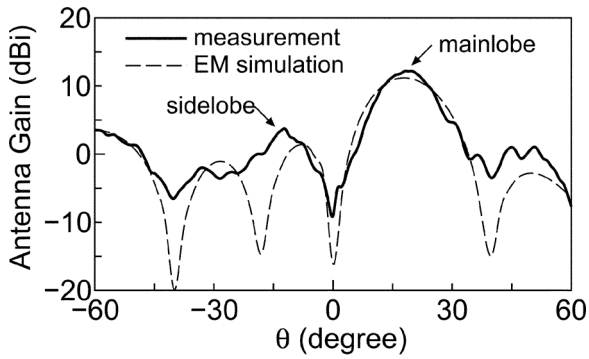

(a)

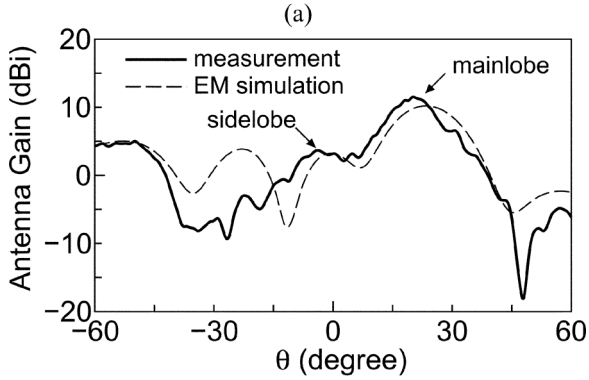

(b)

Fig. 18. Antenna radiation patterns in beam-formed mode. (a) $+18°$. (b) $+24°$. Measurement and EM-simulation methods are same as that of Fig. 1.

Two examples of beam-formed pattern, with the center of the mainlobe aimed at $+18°$ and $+24°$, are shown in Fig. 18. The measured mainlobe directions are well consistent with simulated values. Gain difference between the mainlobe [at $+19°$ in (a)] and Q-omni [at $0°$ in Fig. 1(b)] is 9.3 dB, which is sufficiently within the dynamic range of RX. This ensures reception in the linear region for any antenna patterns without using automatic gain control (AGC) function. Several considerable sidelobes are present. The highest-level sidelobe in (b) is around $0°$ with a gain of 7.8 dB lower than the mainlobe. Effects of these sidelobes will be discussed experimentally in the Section VII-D.

C. Experimental Setup

Fig. 19 shows the measurement setup for BF training experiments. As a training signal, a 100 MHz CW (continuous wave) was input to the TX IF terminal. The signal level was determined so that TX could be operated in its linear region whereas RX could receive signals sufficiently above a noise floor. RF frequency was 60.58 GHz. The RX IF output (100 MHz) level, linearly related to RX received power, was measured in MIDC process and blocker-insertion experiment. The RX amplifiers' gain settings were determined to maintain the RX in linear operation for all antenna settings without using AGC function.

The propagation environment is illustrated in Fig. 20. The TX and RX were placed with an interval of 1.32 m (LOS link distance, indicated by a solid line). One NLOS link (indicated by a dashed line) was constructed by placing a reflector (metal plate). The angle between LOS and NLOS links is represented by ϕ_{NLOS}. In blocker-insertion experiments, a blocker (metal plate) was placed at the center between TX and RX, while the blocker was absent in the MIDC process. Reflections on walls and floors were prevented by EM-wave absorbers. A photograph of the propagation environment is shown in Fig. 21.

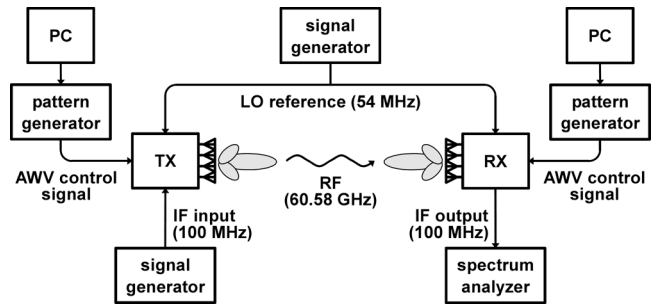

Fig. 19. Measurement setup for beamforming-training experiment. In TX/RX, a 60.48 GHz LO signal is generated from a 54-MHz reference signal by a 30.24-GHz-band phase locked loop (PLL, with frequency division ratio of 1/560) and a 30/60-GHz band frequency doubler. LO signal is then mixed with 100 MHz IF to obtain 60.58-GHz RF signals (TX), or vice versa (RX).

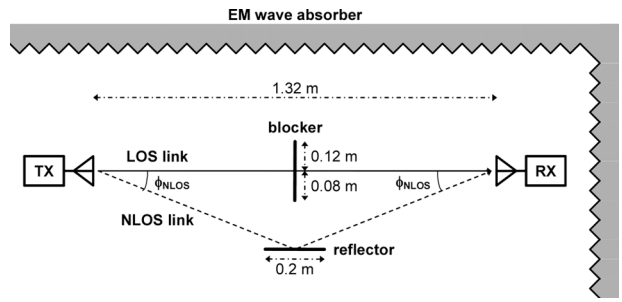

Fig. 20. Propagation environment (schematic).

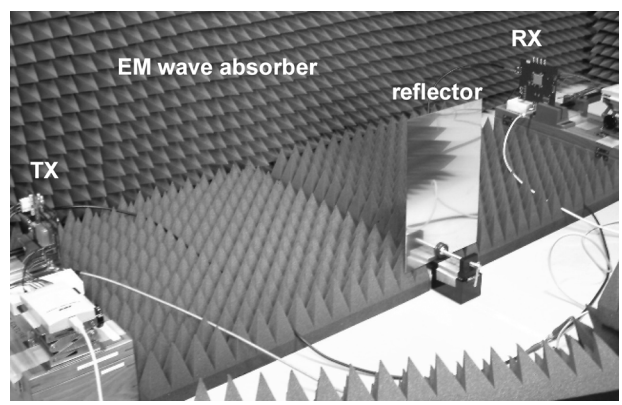

Fig. 21. Propagation environment (photograph). Blocker is not placed in this photo.

D. BF Training and Blocker-Insertion Experiment

We present the experimental results using two different ϕ_{NLOS} values ($23.5°$ and $18°$) for two purposes. First is to show that one peak in the angle profile is surely induced by the NLOS signal, by confirming that the peak angle alters according to ϕ_{NLOS}. Second is to demonstrate various phenomena such as a reversal of LOS and NLOS peak levels in the angle profile owing to the imperfect Q-omni pattern.

1) $\phi_{\mathrm{NLOS}} = 23.5°$ *Case:* Fig. 22 shows the SLS/MID results. In both profiles, a peak corresponding to the LOS direction (TXP1, RXP1 at $0°$) and a peak almost coincident with the

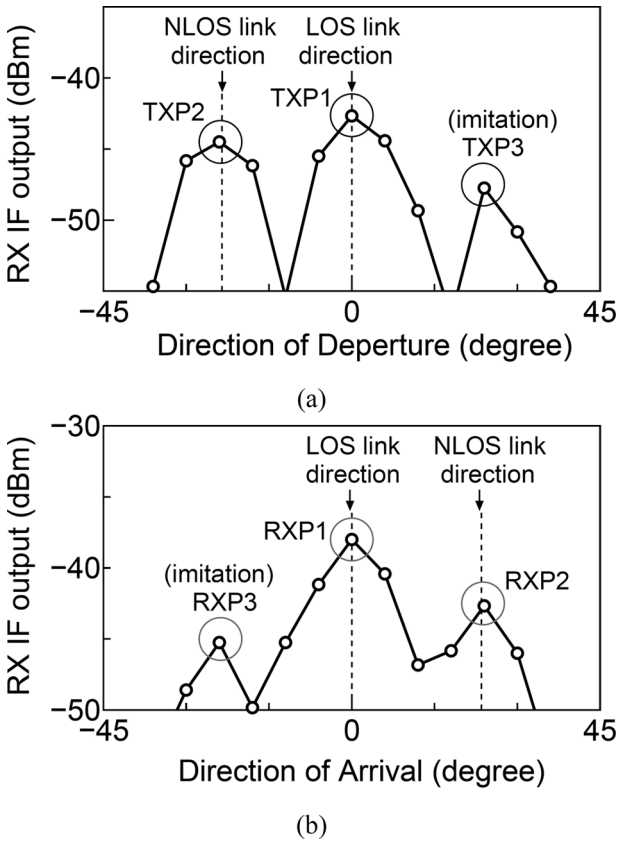

Fig. 22. Angle (Rx-IF-output versus DoA/DoD) profile ($\phi_{\mathrm{NLOS}} = 23.5°$). (a) SLS (TX beam scan). (b) MID (RX beam scan). Peaks were simply detected by searching points at which the derivative changes its sign. In more complicated cases, noise-rejection or smoothing techniques would be needed.

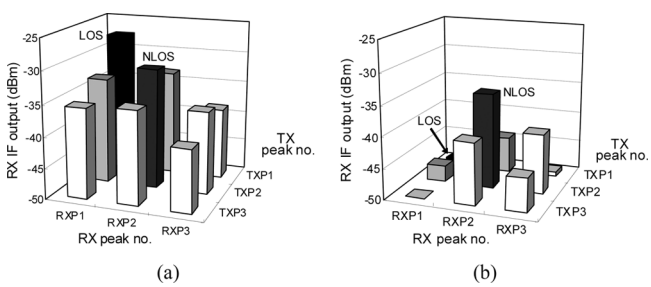

Fig. 23. Results of BC and blocker-insertion experiment ($\phi_{\mathrm{NLOS}} = 23.5°$). (a) Beam Combining (without blocker). (b) Blocker-insertion experiment.

NLOS direction (TXP2, RXP2 at $\pm 24°$) were clearly detected. In addition, third peaks due to sidelobes ("imitation peaks") were detected (TXP3, RXP3). These imitation peaks are considered to be generated by the detection of LOS signals by the sidelobe at $0°$ depicted in Fig. 18(b).

Fig. 23(a) schematically depicts BC results. Three scale points in the x- and y-axes correspond to the peaks with the same legend in Fig. 22. The black and dark-grey pillars indicate the RX IF output for the LOS and NLOS links (corresponding to LOS-LOS and NLOS-NLOS beam pairs), respectively. Here, "(N)LOS beam" is defined as one whose mainlobe is directed to the (N)LOS link. The RX IF output for the NLOS link is 3.5-dB lower than that for the LOS link. Meanwhile, two light-gray pillars express results for "wrong pairs" (LOS-NLOS and NLOS-LOS beam pairs). White pillars are for the pairs where one or both are related to imitation peaks.

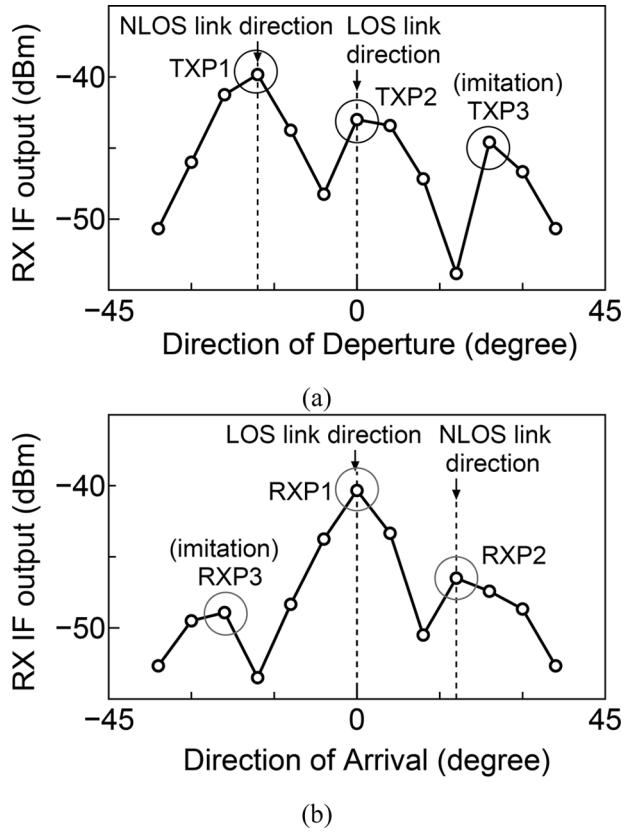

Fig. 24. Angle (Rx-IF-output versus DoA/DoD) profile ($\phi_{\mathrm{NLOS}} = 18.0°$). (a) SLS (TX beam scan). (b) MID (RX beam scan).

Fig. 23(b) shows results when the LOS link was blocked by a metal plate (see Fig. 20). By inserting the blocker, the RX IF output for the LOS link was reduced by over 20 dB whereas it was only 3.5 dB for NLOS link[5,6]. This result indicates that the property of the reserved link is not seriously changed when another link is blocked, thanks to the quasi-optical nature of MMWs. The RX IF outputs for "wrong pairs" were also greatly reduced, because these pairs use the LOS link as illustrated in Fig. 11(a).

2) $\phi_{\mathrm{NLOS}} = 18.0°$ *Case:* Fig. 24 shows the result of another SLS/MID situation. In this case, the levels of LOS peak (TXP2) and NLOS peak (TXP1) in SLS were reversed. This can be mainly attributed to the imperfectness of the Q-omni pattern. Two reasons can be listed as to why such a reversal occurred in this case and not in the $\phi_{\mathrm{NLOS}} = 23.5°$ case. First, difference in the path loss as well as TX antenna gain in beam-formed mode between LOS and NLOS links is smaller in this case. Second, the Q-omni pattern has a peak near $+18°$ as shown in Fig. 1(b). As a result, gain of the Q-omni pattern at $+18°$ becomes 3.3-dB

[5]The knife-edge diffraction loss calculated by considering diffractions at left, right, and top edges of the blocker based on [50] is about 20 dB. This is well consistent with the measured LOS-link RX IF output reduction.

[6]If we change the blocker size, this LOS-link suppression value will change following the knife-edge diffraction loss formula [50], because the blocker is not fully larger than the first Fresnel zone radius (0.041 m in this case). On the other hand, NLOS link characteristics will not largely change because the NLOS link and the blocker are sufficiently apart from each other as compared to the radius.

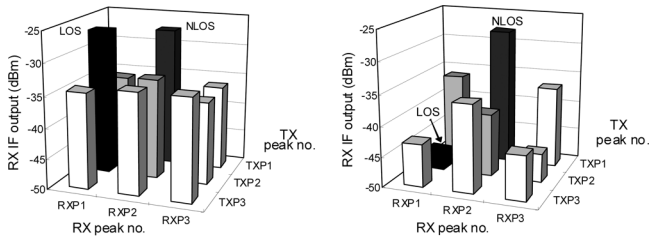

Fig. 25. Results of BC and blocker-insertion experiment ($\phi_{\mathrm{NLOS}} = 18.0°$). (a) Beam Combining (without blocker). (b) Blocker-insertion experiment.

higher than that at 0°. This facilitates the reversal because RX received the signal at this peak of the Q-omni pattern on measuring the RX IF output of TXP1. If TX and RX beams were paired in order of peak level without BC in such a case, a wrong beam combination would be made (e.g., TXP1 and RXP1).

Fig. 25(a) shows the BC results. By executing BC, correct combinations, corresponding to the LOS (TXP2 and RXP1) and NLOS (TXP1 and RXP2) links, were chosen as the upper-two pairs. If the wrong combination (TXP1 and RXP1) was made without BC, about 10 dB link gain would be lost. If the iterative method was applied, TXP1 would be firstly selected in SLS and then NLOS pair (TXP1 and RXP2) would be selected as the best one. As a result, about 1 dB link gain would be lost. This is a symbolic example indicating effectiveness of MIDC experimentally. Fig. 25(b) shows the results of blocker-insertion experiment. The RX IF output for the LOS link was reduced by over 20 dB whereas it was only 0.5 dB for the NLOS link.

E. Summary of Experiments

The above results verify MIDC from the perspective of MMW propagation characteristics. However, they are preliminary and require the following as future work: 1) experiments using wideband modulation signal instead of CW [23], [38], [51], 2) experiments at other MMW frequency bands, 3) experiments in more realistic propagation environments, and 4) AWV control by automatic operation which will enable direct BF-duration estimation.

VIII. Conclusion

A novel BF protocol MIDC has been proposed for 60-GHz band WLAN/PAN systems. MIDC enables to precisely detect the best link even with imperfect Q-omni patterns, and further to reserve multiple antenna settings corresponding to communication links in the initial training by utilizing the quasi-optical nature of millimeter-waves (MMWs). By the latter function, fast beam switching can be accomplished when link blockage occurs. The training can be executed in short duration by putting together DoA/DoD estimation and BC techniques. The basic function of MIDC has been verified experimentally in a simple multipath propagation environment by using 60-GHz CMOS transceiver LSIs and PAAs. MIDC has been adopted in MAC/PHY specifications of primary 60-GHz band standards: WiGig and IEEE 802.11ad, and is a promising candidate for BF protocols in the MMW frequency range including frequencies other than 60 GHz.

Acknowledgment

The authors would like to thank M. Ito, A. Tanaka, Y. Hamada, Z. Yamazaki, and H. Ishikawa for CMOS LSI development, T. Kimura and T. Miyamoto for experimental verification. The authors would also like to thank M. Fukaishi, M. Okada, S. Tanaka, Y. Mochizuki, N. Nishi, H. Shimawaki, M. Ikekawa, K. Kunihiro, S. Tsumura, and Y. Nakamura for their support and encouragement through this work and the editors and reviewers for their valuable comments.

References

[1] S.-K. Yong, P. Xia, and A. V. Garcia, *60 GHz Technology for Gbps WLAN and WPAN: From Theory to Practice*. New York, NY, USA: Wiley, 2010.
[2] T. S. Rappaport, J. N. Murdock, and F. Gutierrez, "State of the art in 60-GHz integrated circuits and systems for wireless communications," *Proc. IEEE*, vol. 99, no. 8, pp. 1390–1436, Aug. 2011.
[3] C. J. Hansen, "WiGiG: Multi-gigabit wireless communications in the 60 GHz band," *IEEE Commun. Mag.*, vol. 18, no. 6, pp. 6–7, Dec. 2011.
[4] [Online]. Available: http://www.wi-fi.org/
[5] [Online]. Available: http://www.ieee802.org/11/Reports/tgad_update.htm
[6] C. Cordeiro, D. Akhmetov, and M. Park, "IEEE 802.11ad: Introduction and performance evaluation of the first multi-Gbps WiFi technology," in *Proc. Int. Workshop mmWave Commun.: From Circuits to Networks (mmCom '10)*, Chicago, IL, USA, Sep. 2010, pp. 3–8.
[7] [Online]. Available: http://www.ieee802.org/15/pub/TG3c.html
[8] [Online]. Available: http://www.wirelesshd.org/
[9] [Online]. Available: http://www.ecma-international.org/default.htm
[10] H. Singh, J. Oh, C. Kweon, X. Qin, H.-R. Shao, and C. Ngo, "A 60 GHz wireless network for enabling uncompressed video communication," *IEEE Commun. Mag.*, vol. 46, no. 12, pp. 71–78, Dec. 2008.
[11] S. Kishimoto, N. Orihashi, Y. Hamada, M. Ito, and K. Maruhashi, "A 60-GHz band CMOS phased array transmitter utilizing compact baseband phase shifters," in *IEEE Radio Frequency Integrated Circuits (RFIC) Symp. Dig.*, Boston, MA, USA, Jun. 2009, pp. 215–218.
[12] A. Valdes-Garcia, S. T. Nicolson, J. W. Lai, A. Natarajan, P.-Y. Chen, S. K. Reynolds, J.-H. C. Zhan, D. G. Kam, D. Liu, and B. Floyd, "A fully integrated 16-element phased-array transmitter in SiGe BiCMOS for 60-GHz communications," *IEEE J. Solid-State Circuits*, vol. 45, no. 12, pp. 2757–2773, Dec. 2010.
[13] M. Fujishima, "Recent trends and future prospective on millimeter-wave CMOS circuits," *IEICE Electron. Express*, vol. 6, no. 11, pp. 721–735, Jun. 2009.
[14] J. Wang, Z. Lan, C.-W. Pyo, T. Baykas, C.-S. Sum, M. A. Rahman, J. Gao, R. Funada, F. Kojima, H. Harada, and S. Kato, "Beam codebook based beamforming protocol for multi-Gbps millimeter-wave WPAN systems," *IEEE J. Sel. Areas Commun.*, vol. 27, no. 8, pp. 1390–1399, Oct. 2009.
[15] L. Chen, Y. Yang, X. Chen, and W. Wang, "Multi-stage beamforming codebook for 60GHz WPAN," in *6th Int. ICST Conf. Commun. and Netw. China (CHINACOM)*, Harbin, China, Aug. 2011, pp. 361–365.
[16] L. Zhou and Y. Ohashi, "Efficient codebook-based mimo beamforming for millimeter-wave WLANs," in *Proc. IEEE 23rd Int. Symp. Personal, Indoor Mobile Radio Commun. (PIMRC)*, Sydney, Australia, Sep. 2012, pp. 1885–1889.
[17] B. Neekzad, J. S. Baras, and K. Sayrafian-Pour, "Energy efficient millimeter wave radio link establishment with smart array antennas," in *Defense Tech. Inf. Center, ADA481336*, Nov. 2006, pp. 1–6.
[18] D. A. Fittipaldi, S. Skafidas, and M. Luise, "IEEE 802.15.3c medium access controller throughput for phased array systems," in *Proc. 18th Annu. IEEE Int. Symp. Personal, Indoor, Mobile Radio Commun. (PIMRC'07)*, Athens, Greece, Sep. 2007, pp. 1–5.
[19] X. An, C.-S. Sum, R. V. Prasad, J. Wang, Z. Lan, J. Wang, R. Hekmat, H. Harada, and I. G. Niemegeers, "Beam switching support to resolve link-blockage problem in 60 GHz WPANs," in *20th IEEE Int. Symp. Personal, Indoor, Mobile Radio Commun. (PIMRC'09)*, Tokyo, Japan, Sep. 2009, pp. 390–394.
[20] B. Li, Z. Zhou, W. Zou, X. Sun, and G. Du, "On the efficient beamforming training for 60GHz wireless personal area networks," *IEEE Trans. Wireless Commun.*, vol. 12, no. 2, pp. 504–515, Feb. 2013.

[21] M. Fakharzadeh, M.-R. N.-Ahmadi, B. Biglarbegian, J. A.-Shokouh, and S. S.-Naeini, "CMOS phased array transceiver technology for 60 GHz wireless applications," *IEEE Trans. Antennas Propag.*, vol. 58, no. 4, pp. 1093–1104, Apr. 2010.
[22] N. Celik, M. F. Iskander, R. Emrick, S. J. Franson, and J. Holmes, "Implementation and experimental verification of a smart antenna system operating at 60 GHz band," *IEEE Trans. Antennas Propag.*, vol. 56, no. 9, pp. 2790–2800, Sep. 2008.
[23] N. Celik, M. F. Iskander, and Z. Zhang, "Experimental verification of the hybrid smart antenna algorithm with modulated waveforms," *IEEE Antennas Wireless Propag. Lett.*, vol. 8, pp. 236–239, Feb. 2009.
[24] C.-S. Choi, M. Elkhouly, E. Grass, and C. Scheytt, "60-GHz adaptive beamforming receiver arrays for interference mitigation," in *Proc. IEEE 21st Int. Symp. Personal, Indoor, Mobile Radio Commun. (PIMRC)*, Istanbul, Turkey, Sep. 2010, pp. 762–767.
[25] *IEEE standard for information technology—telecommunications and information exchange between systems—local and metropolitan area networks—specific requirements. Part 15.3: wireless medium access control (MAC) and physical layer (PHY) specifications for high rate wireless personal area networks (WPANs) amendment 2: millimeter-wave-based alternative physical layer extension*, IEEE Computer Society, Oct. 2009.
[26] Wireless Gigabit Alliance, Inc., WiGiG MAC and PHY specification, version 1.2 Mar. 2013.
[27] *IEEE standard for information technology—telecommunications and information exchange between systems—local and metropolitan area networks—specific requirements. Part 11: wireless lan medium access control (MAC) and physical layer (PHY) specifications, amendment 3: enhancements for very high throughput in the 60 GHz band*, IEEE Computer Society, Dec. 2012.
[28] K. Ramachandran, N. Prasad, K. Hosoya, K. Maruhashi, and S. Rangarajan, "Adaptive beamforming for 60 GHz radios: Challenges and preliminary solutions," in *Proc. Int. Workshop mmWave Commun.: From Circuits to Netw. (mmCom '10)*, Chicago, IL, USA, Sep. 2010, pp. 1–5.
[29] P. F. M. Smulders, "Statistical characterization of 60-GHz indoor radio channels," *IEEE Trans. Antennas Propag.*, vol. 57, no. 10, pp. 2820–2829, Oct. 2009.
[30] H. Xu, V. Kukshya, and T. S. Rappaport, "Spatial and temporal characterization of 60 GHz indoor channels," in *Proc. IEEE-VTS Fall 52nd Veh. Technol. Conf. 2000 (VTC '00)*, Boston, MA, USA, Sep. 2000, vol. 1, pp. 6–13.
[31] H. T. Friis, "A note on a simple transmission formula," *Proc. I.R.E. and Waves and Electrons*, pp. 254–256, May 1946.
[32] T. Derham, "Multiple antenna processing and spatial reuse in 60 GHz wireless PAN/LAN," in *The 20th IEEE Int. Symp. Personal, Indoor and Mobile Radio Commun. (PIMRC'09)*, Tokyo, Japan, Sep. 2009, pp. 1–3.
[33] A. Bourdoux, J. Nsenga, W. V. Thillo, F. Horlin, and L. V. d. Perre, "Air interface and physical layer techniques for 60 GHz WPANs," in *Proc. IEEE Symp. Commun. Veh. Technol.*, Liege, Belgium, Nov. 2006, pp. 1–6.
[34] M. Park, P. Gopalakrishnan, and R. Roberts, "Interference mitigation techniques in 60 GHz wireless networks," *IEEE Commun. Mag.*, pp. 34–40, Dec. 2009.
[35] M. Ueba, A. Miura, S. Kitazawa, S. Saito, and T. Ohira, "Feasibility study on millimeter wave multi-gigabit wireless LAN system," in *Proc. IEEE Eur. Microw. Conf.*, Munich, Germany, Oct. 2007, pp. 688–690.
[36] T. Manabe, Y. Miura, and T. Ihara, "Effects of antenna directivity and polarization on indoor multipath propagation characteristics at 60 GHz," *IEEE J. Sel. Area Commun.*, vol. 14, no. 3, pp. 441–448, Apr. 1996.
[37] M. S. Choi, G. Grosskopf, D. Rohde, B. Kuhlow, G. Przyrembel, and H. Ehlers, "Experiments on DOA-estimation and beamforming for 60 GHz smart antennas," in *Proc. 57th IEEE Semiannu. Veh. Technol. Conf., (VTC '03-Spring)*, Jeju, Korea, Apr. 2003, pp. 1041–1045.
[38] A. Maltsev, R. Maslennikov, A. Sevastyanov, A. Khoryaev, and A. Lomayev, "Experimental investigations of 60 GHz WLAN systems in office environment," *IEEE J. Select. Areas Commun.*, vol. 27, no. 8, pp. 1488–1499, Oct. 2009.
[39] M. Flament and A. Svensson, "Virtual cellular networks for 60 GHz wireless infrastructure," in *Proc. IEEE Int. Conf. Commun. (ICC'03)*, Anchorage, AK, USA, May 2003, pp. 1223–1227.
[40] Z. Fan, "Wireless networking with directional antennas for 60 GHz systems," in *Proc. 14th Eur. Wireless Conf. 2008 (EW '08)*, Prague, Czech Republic, Jun. 2008, pp. 1–7.
[41] P. Sanchis, V. Polo, J. Herrera, J. L. Corral, M.-S. Choi, and J. Marti, "Experimental demonstration of a direction-of-arrival estimation algorithm for millimeter-wave switched-beam array antennas," *Microw. Opt. Technol. Lett.*, vol. 39, no. 3, pp. 199–201, Nov. 2003.
[42] S.-S. Jeon, J.-Y. Park, Y. Wang, and T. Itoh, "A broadband beamformer for millimeter-wave systems using sub-band sampling," in *IEEE MTT-S Int. Microw. Symp. Dig.*, Philadelphia, PA, USA, Jun. 2003, pp. 579–582.
[43] M.-S. Lee, J.-Y. Park, V. Katkovnik, T. Itoh, and Y.-H. Kim, "Adaptive robust DOA estimation for a 60-GHz antenna-array system," *IEEE Trans. Veh. Technol.*, vol. 56, no. 5, pp. 3231–3237, Sep. 2007.
[44] [Online]. Available: http://www.ansys.com/
[45] T. Hao Ngoc, J. Takagi, H. Oguma, S. Kameda, H. Nakase, T. Takagi, and K. Tsubouchi, "Indoor multipath propagation characteristics at 60GHz," in *Proc. IEEE Region 10 Conf. (TENCON '06)*, Hong Kong, China, Nov. 2006, pp. 1–4.
[46] H.-R. Shao and C. Ngo, "Method and system for communication of uncompressed video information in wireless systems, , ," United States Patent Application Publication US 2009/0021646 A1, Jan. 22, 2009.
[47] Z. Chen, G. Gokeda, and Y. Yu, *Introduction to direction-of-Arrival estimation*. Norwell, MA, USA: Artech House, 2010.
[48] K. Hosoya, K. Maruhashi, and N. Orihashi, "Control method of wireless communication system, wireless communication system, adjustment method of array weight vector, and wireless communication device," U.S. patent, US 8508409 B2, Aug. 13, 2013.
[49] IEEE P802.15 Working Group for Wireless Personal Area Networks (WPANs), TG3c channel modeling sub-committee final report, IEEE 15–07–0584–01–003c 2007.
[50] Rec. ITU-R P.526-8, Propagation by diffraction, question ITU-R 202/3 1978–1982–1992–1994–1995–1997–1999–2001–2003.
[51] A. S. Ioffe and M. S. Stoytchev, "Wideband channel measurements and characterization of the wireless home environment," in *Proc. IEEE Antennas Propag. Soc. Int. Symp.*, Albuquerque, NM, USA, Jul. 2006, pp. 3077–3080.

Ken'ichi Hosoya (M'98) received the B.A. degree in pure and applied science and the Ph.D. degree in engineering, both from the University of Tokyo, Tokyo, Japan, in 1991 and 2009, respectively.

In 1991, he joined NEC Corporation, Kawasaki, Japan, where he has been engaged in the development of millimeter-wave GaAs high electron mobility transistors (HEMTs) and their microwave monolithic integrated circuits (MMICs) for 60-GHz-band wireless communication systems, GaAs heterojunction bipolar transistor (HBT) MMICs for 77-GHz-band automotive radar systems, and ultra-high-speed ICs for 40-Gbps optical communication systems based on GaAs HBTs, InP HBTs, and CMOS. He is currently a Principal Researcher with Green Platform Research Laboratories, NEC Corporation. His research interests include beamforming techniques for millimeter-wave wireless local/personal area networks (WLAN/PANs) and mobile backhauls.

Dr. Hosoya is a member of the Institute of Electronics, Information and Communication Engineers (IEICE), Japan. He was awarded APMC'99 Microwave Prize presented at 1999 Asia Pacific Microwave Conference, Singapore.

Narayan Prasad received the B.Tech. degree in electrical engineering from the Indian Institute of Technology, New Delhi, India, in 1999, and the Ph.D. degree in electrical and computer engineering from the University of Colorado, Boulder, CO, USA, in 2004.

He is currently a Senior Researcher at NEC Laboratories America, Princeton, NJ, USA. His research interests include multi-user space-time communications, information theory, and radio resource management.

Kishore Ramachandran received the Ph.D. degree in computer engineering from Rutgers University, New Brunswick, NJ, USA, in 2009.

He is cofounder of Zipreel, Inc. (a start-up focused on large-scale media processing) and also serves as its Chief Executive Officer. He is responsible for Zipreel's overall strategy, technology R&D, and engineering operations. Prior to Zipreel, he was with NEC Labs America, Inc., where his work on enhancing datacenter networks with wireless (millimeter-wave) interconnects led to multiple patents and IEEE standards contributions. He has been issued six patents so far.

Naoyuki Orihashi received the B.S. degree in physics from Chuo University, Tokyo, Japan, in 2001 and the M.E. and D.E. degrees in information processing from Tokyo Institute of Technology, Tokyo, Japan, in 2003 and 2006, respectively.

In 2006, he joined the NEC Corporation, Kawasaki, Japan. His research interest includes development of antennas and passive devices of millimeter-wave and microwave for high-speed wireless communication and sensor applications.

Dr. Orihashi received a JJAP Paper Award in 2006 from the Japan Society of Applied Physics.

Shuya Kishimoto (M'03) received the B.E., M.E., and Dr.Eng. degrees in electronic engineering from Tohoku University, Sendai, Japan, in 1995, 1997, and 2000, respectively.

In 2001, he joined the NEC Corporation, Kawasaki, Japan. His research interest includes development of millimeter-wave CMOS phased array transceivers for high-speed wireless communication and sensor applications.

Dr. Kishimoto is a member of the Institute of Electronics, Information and Communication Engineers of Japan (IEICE).

Sampath Rangarajan (M'91–SM'05) received the Ph.D. degree in computer science from the University of Texas, Austin, TX, USA.

He heads the Mobile Communications and Networking Research Department at NEC Laboratories America in Princeton, NJ, USA. Previously, he was with the Networking Research Center at Bell Laboratories in Holmdel, NJ. Prior to that, he was cofounder and vice president of technology at Ranch Networks, a venture funded startup in the IP networking space. Earlier, he was a researcher in the Systems and Software Research Center at Bell Laboratories in Murray Hill, NJ. Before joining Bell Laboratories, he was an Assistant Professor in the Electrical and Computer Engineering Department at Northeastern University, Boston, MA, USA. His research interests span the areas of mobile communications, mobile networks, and distributed systems.

Dr. Rangarajan is a senior member of the IEEE and has been on the editorial boards of IEEE TRANSACTIONS ON COMPUTERS, IEEE TRANSACTIONS ON PARALLEL AND DISTRIBUTED SYSTEMS, and *ACM Mobile Computing and Communications Review*.

Kenichi Maruhashi (M'95) received the M.S. degree from Kobe University, Kobe, Japan, in 1991 and the Ph.D. degree from and Tohoku University, Sendai, Japan, in 1991 and 2007, respectively.

After joining NEC Corporation in 1991, he worked on the developments of GaAs-based low-noise FETs, GaAs- and CMOS-based millimeter-wave integrated circuits, modules and sub-systems followed by engaging in millimeter-wave standardization. He is now a Senior Manager of NEC Smart Energy Research Labs., where he conducts the research and development of Li-ion battery systems and controlling technology as well as energy management systems.